www.czasopisma.pan.pl PAN www.journals.pan.pl
Chemical and Process Engineering 2019, 40 (4), 377–397
DOI: 10.24425/cpe.2019.130213

NUMERICAL SIMULATION OF DEFORMATION AND FRAGMENTATION OF FRACTAL-LIKE NANOAGGREGATES

Łukasz Żywczyk[1], Arkadiusz Moskal[2], Rafał Przekop[2,*]

[1] Polish Academy of Sciences, Institute of Fundamental Technological Research,
ul. Pawińskiego 5B, 02-106 Warsaw, Poland
[2] Warsaw University of Technology, Faculty of Chemical and Process Engineering,
ul. Waryńskiego 1, 00-645 Warsaw, Poland

A flexible fractal-like aggregate model was used to study deformation and fragmentation of the structure of fractal-like aggregates via their impaction with rigid rough surface. Aggregates were conveyed one at the time towards a surface under vacuum conditions. The number of primary particles remaining in each fragment, ratio of average fragment radius of gyration after impaction to the average fragment initial radius of gyration and ratio of average coordination number to the initial coordination number were monitored for each individual aggregate. Results demonstrate that depending on the impact velocity, the fractal dimension of the aggregate, the strength of bonds between primary particles, the stiffness of the aggregate structure and the diameter of primary particle composing an aggregate, restructuring or breakage of the aggregate occur. Moreover, in the analysis of the ratio of coordination number of aggregates after impaction to the initial coordination number, three regimes were distinguished: first no deformation at low impact velocities, second restructurisation regime and finally fragmentation regime where partial or total fragmentation of aggregates was observed.

Keywords: fractal-like aggregate, discrete element modelling, fragmentation, restructuration

1. INTRODUCTION

Investigating the structure breakup of aggregated particles plays a significant role in the chemical and pharmaceutical industries, where careful control of the impact breakage of aggregates provides the source of nanoparticle aerosol (Grzybowski et al., 2009) for new materials like catalysts or electrical sensors (Strobel and Pratsinis, 2007). However, one can look as well into the restructuring of aggregate structures during impact, which can lead to formation of structures with the desired morphology (Ilmura et al., 1998). The question arises whether the initial velocity of the aggregate will guarantee complete de-aggregation of its structure or the aggregate will be restructured. Another question is how the morphology of aggregates and the strength of bonds between primary particles determine the degree of aggregate breakage. It is possible to understand the mechanical stability of such structures by investigating collision of aggregates with a rigid obstacle (Froeschke et al., 2003). Understanding how different factors can influence the breakage of the structure of an aggregate is mandatory from the perspective of process optimisation.

Research on the breakage of aggregate structures must be enhanced by theoretical modelling using mathematical models that enable to investigate different factors, which influence restructuration and fragmentation.

* Corresponding author, e-mail: rafal.przekop@pw.edu.pl

Theoretical studies over the fragmentation of aggregate structures provide important information which would be not accessible via laboratory investigation. Thornton et al. (1996) used Discrete Element Modelling (DEM) and found that, depending on the values of impact velocities and surface free energy of particles, three regimes of behaviour may be observed; shattering, semi-brittle fracture and elastic rebound. Ilmura et al. (1998) studied deformation of aggregates during their impaction, using modified Discrete Element Modelling (mDEM) approach. They found that at low impact velocities, aggregate modification degree is adequate to the impaction force. Moreno et al. (2003) studied the influence of the impact angle on breakage characteristics of spherical agglomerates. Moreno-Atanasio and Ghadiri (2006) proposed a simple mechanistic model that relates the number of broken contacts in an agglomerate due to impact velocity, interparticle adhesion energy and particle properties. Wittel et al. (2008) employed DEM to study wave energy propagation during agglomerate impaction with a rigid obstacle and mechanisms involved in fragmentation of structures. The very physical and accurate DEM approach has become increasing used in the literature over the past few years and is used to study various processes concerning aggregates (Cundall and Strack, 1979; Dai 2010; Kafui and Thorton, 1993; Tamadondar et al., 2017; Zhang et al., 2019). However, it has not been applied to study fragmentation of fractal-like aggregates. The fact is that fractal-like aggregates, during impaction behave very differently from compacted agglomerates. In order to simplify the description of internal forces, Grzybowski et al. (2009) developed a model of aggregate where interactions between non-contacting particles in the aggregate are described by van der Waals theory, coupled with adhesion forces modelled by Derjaguin et al. (1975) for primary particles in contact. The model takes into account only forces acting in normal direction between connected primary particles. Grzybowski et al. (2009) found that a combination of nano-size particles and micro-size particles differentiate the fragmentation process, which provides necessarily information for structure control size produced by impaction.

As one can see, although there are many different mathematical approaches, most studies involve compacted aggregates (or agglomerates). One wish to distinguish fractal-like aggregate is defined according to Chambers Science and Technology Dictionary (Walker, 1988), as an assemblage of particles, which are loosely coherent. On the other hand an agglomerate is defined as an assemblage of particles rigidly joined together, as by partial fusion (sintering) or by growing together. For that reason, it is necessary to further research to involve fractal-like aggregates with a variety of shapes.

According to state-of-the-art, fragmentation of soft aggregates has never been investigated numerically in the function of fractal dimension of aggregate. The number of studies on the subject is limited. Only experiments conducted by Froeschke et al. (2003) deliver us important information that more compacted aggregates are less breakable because of higher coordination number of primary particles, defined as the number of its immediate neighbours, compared to aggregates with lower fractal dimension. This needs to be verified for a much more wider range of shapes of fractal-like aggregates. Secondly, collision of fractal-like aggregate with rigid surface has never been investigated for low impact velocities. Only results reported by Moreno-Atanasio and Ghadiri (2006) indicate that at low impact velocities, aggregates do not experience any restructuration. We show that aggregates can develop another functional structure when they are impacted with very low velocities. There exist a work of Ilmura et al. (1998), which showed that as aggregate impact velocity rises, the aggregate becomes more compacted. Looking at the average coordination number of primary particles before and after the collision one can monitor this phenomenon. Another factor which has not been investigated and which can influence the behaviour of aggregate after impaction is its stiffness. Aggregate stiffness can strongly influence its restructuration.

The aim of this study was to investigate the subject with a new model, which constitutes an alternative way to simulate the dynamics of complex structures of fractal-like aggregates (Żywczyk and Moskal, 2015). The approach that has been presented in this study offers another mathematical description to study mechanical stability of complicated aggregate structures. The new model can be used to investigate the stability of aggregates under the influence of different factors, such as fractal dimension, constitutive primary particle

diameter, strength of primary particle bonds, structure flexibility as a function of impact kinetic energy. Those factors are often difficult to investigate experimentally and therefore must be addressed in the present study.

2. FLEXIBLE AGGREGATE MODEL (FAM)

2.1. Numerical algorithm for the generation of fractal-like aggregates

Three-dimensional aggregates composed of N identical spheres are considered in the simulation. Irregular, porous structures of aggregates can consist of between a few and thousands of primary particles, ranging between 5 to 100 nm in diameter (Friedlander, 2000). To cover a large range of shapes and sizes of aggregates in the simulation, populations of aggregates composed of the numbers of primary spherical particles of $N = 40$, were generated using the Diffusion Limited Aggregation *(DLA)* algorithm (Witten and Sander, 1981). Some generated structures are depicted in Fig. 1.

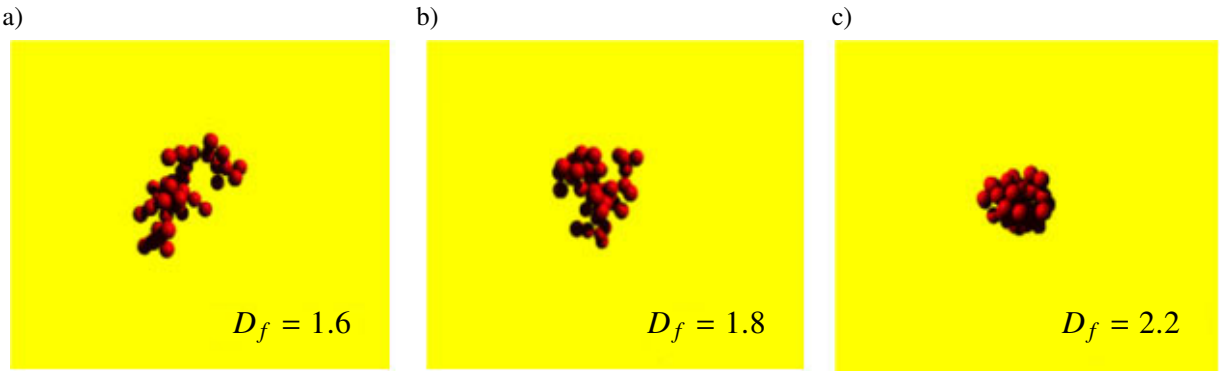

Fig. 1. Various configurations of the generated fractal-like aggregates ($N = 40$, $d_p = 20$ nm)

Particle-cluster aggregation was used to generate a variety of aggregates with different fractal forms. Each population, varied with D_f contained ten different aggregates. The following procedure was used, which is only briefly described here. A seed particle is placed in the centre of a sphere, denoted here as the control volume with a chosen radius. The adjoining particles are randomly generated at the edge of the control volume, and their movement towards the centre of the control volume is described by the Brownian dynamics (BD) equations (Bałazy and Podgórski, 2007). A particle is assumed to be attached to the structure when the distance between joined particles is less than the diameter of the primary particle, as defined in the procedure. The fractal dimension of the created aggregate will depend on the chosen radius of the control volume sphere. Each of the subsequently generated aggregates has different features from other aggregates in the population. Note that particles moved in the air, whose temperature and viscosity were 293.15 K and 1.821×10^{-5} Pa·s, respectively. The time step used to integrate BD equations was two orders of magnitude smaller than relaxation time of particle with diameter d_p. Relaxation time was calculated using Eq. (1):

$$\tau = \frac{\rho_p d_p^2 C_c}{18\mu} \tag{1}$$

where ρ_p and d_p are density and diameter of the primary particle, respectively, and C_C is the Cunningham slip correction factor expressed by:

$$C_c = 1 + Kn\,[1.257 + 0.4\exp(-0.55Kn)] \tag{2}$$

where Kn is the Knudsen number based on particle diameter. Cunningham factor becomes more significant for a smaller particle and when mean free path of gas molecules becomes greater and accounts for the slip condition, which is more significant when Knudsen number is increasing.

In the simulations, the density of the primary particles used was $\rho_p = 2600$ kg·m^{-3}, and the primary particle diameter used was $d_p = 5$, 10 and 20 nm.

2.2. Equation of motion

To determine the motion of an aggregate and to evaluate its internal forces is a complex mathematical problem. Nevertheless, solving the motion equations for each constituent spherical particle of the aggregate structure can follow the evolution of the aggregate structure. The set of the equations combines translational and rotational Newton's second law of motion.

Conveniently, Eq. (3) represents a sum of all forces contributing to the movement of the i-th particle of an aggregate in a single time step:

$$m_{pi}\frac{dv_i}{dt} = \sum_{i=1}^{N} F_i^s + \sum_{i=1}^{N} F_i^{dpp} + \sum_{i=1}^{N} F_i^b + \sum_{i=1}^{N} F_i^t + \sum_{i=1}^{N} F_i^p + \sum_{i=1}^{N} F_i^{ub} + \sum_{i=1}^{N} F_i^{dub} + \sum_{i=1}^{N} F_i^{ps} + \sum_{i=1}^{N} F_i^{dps} + F_g \quad (3)$$

where m_{pi} and v_i are the mass and velocity of primary particle, respectively. F_i^s, F_i^b, F_i^t, F_i^p are the bond (spring), bending, torsion and inversion internal interaction forces in aggregate structure, F_g is the gravity force, F_i^{ps} surface-particle interaction force, F_i^{ub} is the Urey–Bradley force which supports bending force in each tee configuration and F_i^{dpp} is the damping force of harmonic oscillations between connected particles in an aggregate.

2.3. Model of the inter-particle interaction

Nano-particle chain aggregates (NCA) show properties similar to those of molecular polymers (Friedlander, 1999). This was proved by extensive studies (Friedlander et al., 1998). The aggregate structure can be stretched under tensile stress and, when stress relaxes, the aggregate contracts to its initial shape. However, as indicated by Friedlander (1999) the basic properties of aggregates differ from the properties of polymers. Nevertheless, the mathematical equations that are used to describe molecular polymers can be used to simulate internal interactions between primary particles composing the structure of fractal-like aggregate (Allen and Tildesley, 1987; Gao, 1998).

First, subsequent configurations of primary particles in fractal-like aggregates can be distinguished (Żywczyk and Moskal, 2015):

- Pairs of bonded particles i–j, Fig. 2(a), described by the harmonic bond potential energy function, Eq. (4). Tees (triplets) of particles i–j–k and two pairs of bonded particles, i–j and k–j, connected via one common particle j, Fig. 2(b), described by the harmonic cosine angle potential energy function, Eq. (13).
- Quadruple of particles i–j–k–l and two pairs of bonded particles, i–j and l–k, connected via a middle pair j–k, Fig. 2(c), described by the torsion potential energy function, Eq. (17).
- Quadruple of particles i–j–k–l and triplet of particles i–j–k connected with the last particle l via a bond with the middle particle j, Fig. 2(d), described by the inversion potential energy function, Eq. (22).

Pairs of non-bonded particles i–k, (see Fig. 2(b)), described by the harmonic bond potential energy function, Eq. (26).

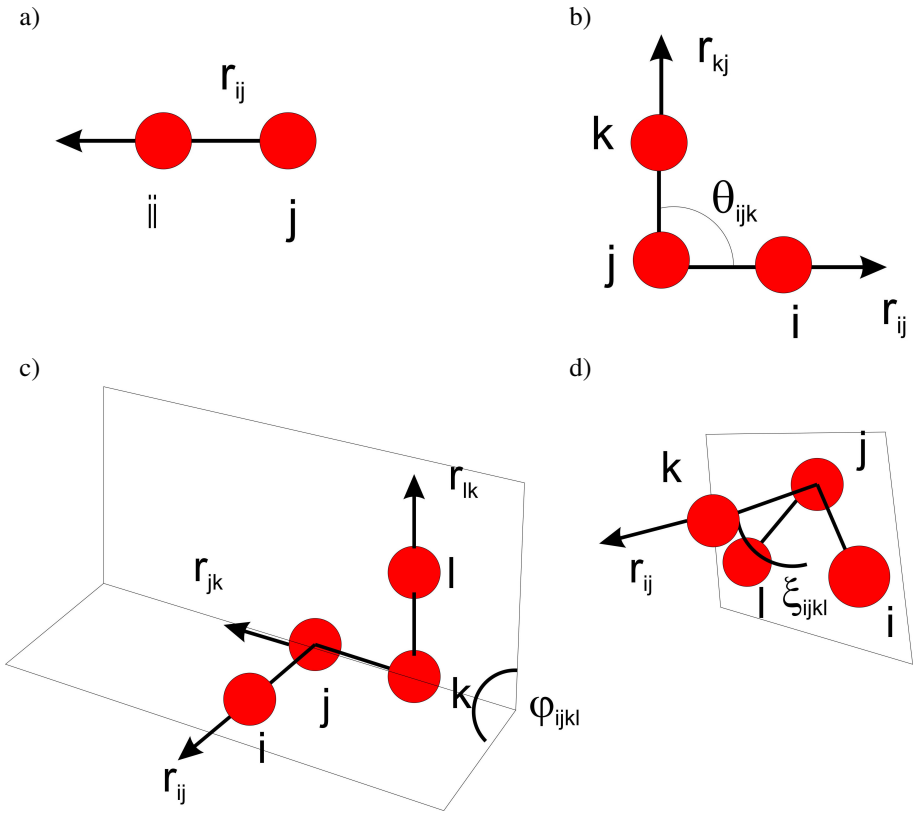

Fig. 2. Various configurations of connected particles in fractal-like aggregates

Functions that describe the interactions between particles in the above-mentioned configurations are represented by five potential energy functions, which will be described below. Those potential energy functions control resistance to any modification of aggregate structure caused by an external factor like impaction with surface.

Interaction forces between pairs of bonded particles depicted in Fig. 2(a) are derived, as a harmonic bond potential energy, V_s, from

$$V_s(r_{ij}) = \frac{1}{2}k_3(r_{ij} - r_{0ij})^2 \tag{4}$$

where k_s is the bond constant, r_{ij} is the distance between geometrical centres of joined particles, and r_{0ij} is the equilibrium distance between geometrical centres of joined particles. Eq. (4) is used to provide the internal force acting in normal direction between joined primary particles. The force derived from Eq. (4) keeps the distance between geometrical centres of connected particles *i–j* close to the value of r_{0ij}. In order to obtain the force acting on *i*-th particle one has to differentiate V_s over the radius of the *i*-th particle:

$$F_i^b = -\frac{\partial V_s(\theta_{ijk})}{\partial r_i} \tag{5}$$

The bond constant k_s in Eq. (4) can be obtained from (Przekop et al., 2004; Vainshtein et al., 1997; Ziskind et al., 2000):

$$k_s = 2.4\left(\gamma\kappa_s^2\frac{d_p^2}{4}\right)^{1/3} \tag{6}$$

where γ is the surface energy between the joined particles. Surface energy is defined by the Dupré equation (Israelachvili, 1985) as:

$$\gamma = \gamma_1 + \gamma_2 - \gamma_{12} \tag{7}$$

where γ_1 and γ_2 are the surface energies of two particles made of different materials which are in contact with each other and γ_{12} is the interaction energy between them. For surfaces of the same material γ_{12}

is zero and therefore interface energy is equal to the sum of surface energies taken from both particles (Moreno-Atanasio and Ghadiri, 2006).

The elastic constant, κ_s, which represents material properties, in Eq. (6) can be calculated using Eq. (8) for two non-identical connected materials (Guingo and Minier, 2008; Przekop et al., 2004):

$$\kappa_s = \frac{4}{3}\left(\frac{1-\nu_{p1}}{Y_{p1}} - \frac{1-\nu_{p2}}{Y_{p2}}\right)^{-1} \tag{8}$$

If the aggregate is composed of particles from the same material and diameter, Eq. (8) reduces to Eq. (9), (Moreno-Atanasio and Ghadiri, 2006):

$$\kappa_s = \frac{2}{3}\left(\frac{1-\nu_p}{Y_p}\right)^{-1} \tag{9}$$

where Y_p is the Young's modulus and ν_p is Poisson's ratio of the material.

The oscillations between primary particles are damped by the force, whose vectors are directed opposite to the relative velocity of i-th particle:

$$F_i^{dpp} = -f_{pp}v_i^{rel} \tag{10}$$

where v_i^{rel} is the relative velocity between connected (neighbouring) particles in an aggregate. Relative velocity is calculated by taking into account only the neighbouring particle of i-th particle. Parameter, f_{pp}, called damping factor is defined as the resistance of the particle-particle mechanical interaction, and it was estimated from (Reeks et al., 1988):

$$f_{pp} = \frac{2.4}{\pi}\frac{m_p k_s^2}{\rho\left(\frac{Y_p}{\rho_p}\right)^{3/2}} \tag{11}$$

where k_s is the "spring" constant.

Apart from forces, which are acting in normal direction between connected particles, other forces contribute to the interactions between joined particles. Pantina and Furst (2005) experimentally demonstrated the existence of tangential forces, which describe bond-bending effects between connected particles. Becker et al. (2009), Cundall (1979), Dominik and Tielens (1997), Ilmura et al. (1998) and Paszun and Dominik (2009) included resistance against sliding (bending) effect between connected primary particles, which can exactly be modelled by tangential forces. In the present model, in order to include resistance against bending, harmonic cosine angle potential energy is implemented. The calculation of bending was performed by Ermak and McCammon (1978) or quite recently by Isella and Drossinos (2011).

The harmonic cosine angle potential energy function, V_b, was used to keep the angle between the pairs of particles i–j and k–j in a tee configuration i–j–k close to equilibrium value θ_{0ijk}:

$$V_b(\theta_{ijk}) = \frac{1}{2}k_b\left[\cos(\theta_{ijk}) - \cos(\theta_{0ijk})\right]^2 \tag{12}$$

where θ_{ijk} is the angle between the vectors i–j and k–j created by the joined particles, k_b is the bending constant. Eq. (12) represents resistance to bending of configuration depicted in Fig. 2(b). The value of the angle θ_{ijk} can be obtained from:

$$\cos(\theta_{ijk}) = \frac{r_{ij}r_{kj}}{|r_{ij}||r_{kj}|} \tag{13}$$

The bending force is given by:

$$F_i^b = -\frac{\partial V_b(\theta_{ijk})}{\partial r_i} \tag{14}$$

The same procedure is applied to particles k in tee configuration. Bending force acting on middle particle j of tee configuration, will equal the negative sum of bending forces acting on i and k particles:

$$F_j^b = -F_i^b - F_k^b \tag{15}$$

In addition, Becker et al. (2009), Dominik and Tielens (1997) and Paszun and Dominik (2009) introduced resistance of connected particles against the internal torsion. In the present model torsion potential energy function was implemented in order to represent resistance forces against torsion of aggregate structure. The torsion potential energy function, V_t, applied to each i–j–k–l quadruple, keeps the angle φ_{ijkl} between the normal vectors of planes created by the triplets of particles i–j–k and j–k–l close to the value φ_{0ijkl}. It represents resistance to torsion of configuration depicted in Fig. 2(c):

$$V_t(\theta_{ijkl}) = \frac{1}{2} k_b \left[\cos(\varphi_{ijkl}) - \cos(\varphi_{0ijkl})\right]^2 \tag{16}$$

where k_t is the torsion constant, φ_{ijkl} is the angle created between the normal vector of the triplet i–j–k particles and the normal vector created from the triplet j–k–l. The angle φ_{ijkl} can be established from:

$$\cos(\varphi_{ijkl}) = \frac{\boldsymbol{A}\,\boldsymbol{B}}{|\boldsymbol{A}||\boldsymbol{B}|} \tag{17}$$

where $\boldsymbol{A}$ and $\boldsymbol{B}$ are the normal vectors of planes created by the vectors of the i–j–k and the j–k–l particles configurations, respectively

$$\boldsymbol{A} = \boldsymbol{r}_{ij} \times \boldsymbol{r}_{jk} \tag{18}$$

$$\boldsymbol{B} = \boldsymbol{r}_{jk} \times \boldsymbol{r}_{kl} \tag{19}$$

The bending force is derived by differentiation as indicated in Eq. (20):

$$F_i^b = -\frac{\partial V_b(\varphi_{ijkl})}{\partial r_i} \tag{20}$$

The interactions in the last configuration of particles depicted in Fig. 2(d) are modelled mathematically by the inversion potential energy:

$$V_t(\xi_{ijkl}) = \frac{1}{2} k_p \left[\cos(\xi_{ijkl}) - \cos(\xi_{0ijkl})\right] \tag{21}$$

where k_p is the inversion constant, ξ_{ijkl} is the angle between the plane created by the triplet of particles i–j–k and the vector created by the particles j–l. This potential energy function prevents this configuration of primary particles, depicted in Fig. 2(d) from inversing into its mirror configuration. Angle ξ_{ijkl} can be established by the following equation, using normal vector $\boldsymbol{A}$ of the plane created by the triplet of particles i–j–k:

$$\sin(\xi_{ijkl}) = \frac{\boldsymbol{A}\,\boldsymbol{r}_{ij}}{|\boldsymbol{A}||\boldsymbol{r}_{ij}|} \tag{22}$$

$$\boldsymbol{A} = \boldsymbol{r}_{ij} \times \boldsymbol{r}_{jk} \tag{23}$$

In the same quadruple configuration, Fig. 2(d), one can observe two more angles: the angle between vector k–j and the plane i–j–l and the angle between the vector i–j and the plane k–j–l. Therefore, the inversion potential energy function involves three angles in the same configuration of four particles. Note that the central particle j can have up to several neighbouring particles. All harmonic functions were differentiated to give adequate forces acting on primary particles composing configurations. A detailed solution can be found in Appendix (Żywczyk and Moskal, 2015).

$$F_i^p = -\frac{\partial V_p(\xi_{ijkl})}{\partial r_i} \tag{24}$$

Apart from the above configurations, another potential function is used in FAM model. In order to support stiffness of the whole aggregate structure, Urey–Bradley spring potential function was imposed between each border k–i particles in the tee configuration, as one will see in Fig. 2(b). Note, that it is not a bond between particles k–i. Urey–Bradley spring potential function is expressed by:

$$V_{ub}(r_{ik}) = \frac{1}{2} k_{ub} \left(r_{ik} - r_{0ik}\right)^2 \tag{25}$$

Where r_{0ik} is the equilibrium distance between particles k–i. Note that Urey–Bradley potential function is differentiated in the same way as the bond potential function represented by Eq. (4). Therefore one has:

$$F_i^{ub} = -\frac{\partial V_{ub}(r_{ik})}{\partial r_i} \tag{26}$$

Note that, the value of $k_{ub} \ll k_s$.

Damping oscillation force imposed on Urey–Bradley force is expressed by:

$$F_i^{dab} = -f_{ub} v_i^{rel} \tag{27}$$

where f_{ub} is estimated by Eq. (11).

Neighbouring particle (also connected or bonded particle) of i-th particle, is defined as a particle whose geometrical centre is located at the distance less than diameter of i-th primary particle. Bond strength is controlled by k_s value. Stiffness (or flexibility) of the aggregate structure is controlled by imposing particular value of constants k_t, k_p, k_b, k_{ub}. In case when the value of the constant is small, appropriate configuration can experience greater excess throughout external excitation. If you increase the value of each constant, each configuration and the whole aggregate stay closer to its equilibrium state.

The order of magnitude of three constants: k_t, k_p, k_b will be considerably smaller than k_s. A similar situation appear in the work of Becker et al. (2009) where torsion constant appears to be a small value with respect to tangential spring stiffness constant or work of Seizinger et al. (2012) where torsion constant is smaller compared to rolling or sliding motion.

3. RESULTS AND DISCUSSION

Calculations were performed using a self-written programme in C++ language. The equation of motion for primary particles was integrated using Runge–Kutta 3rd order method. Restructuration and fragmentation processes of aggregates were investigated numerically by colliding aggregates with a rigid obstacle using flexible fractal-like aggregate approach. From the population of 10 different aggregates with a particular D_f each individual aggregate was directed to collide perpendicularly with the rigid surface, one at a time. This procedure was repeated 100 times for each individual aggregate. Each aggregate was composed of $N = 40$ primary particles. Before the aggregate was moved towards the surface, its structure was rotated around an arbitrary axis, in order to generate different relative orientation to the surface. There were no aggregate structural changes before its collision with the obstacle. Simulation time for each individual aggregate was sufficient in order to follow structural changes during the collision. In order to cut down computational time for each realization, the structure of the aggregate was suspended at a distance of one half of the diameter of primary particle, between the surfaces of the particle located at the lowest position of the aggregate. Aggregates composed of spherical particles of the same diameter collided with the surface composed of primary particles with the diameter $d_p/4$, Fig. 3. Note, that aggregates where conveyed in vacuum, towards a rigid rough surface.

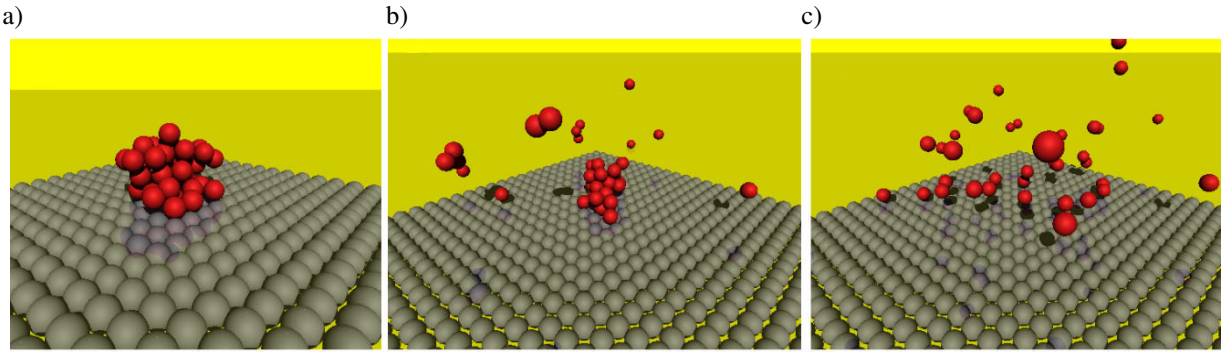

Fig. 3. Snapshots of aggregate collision with surface with impact velocity $U = 10$ m/s

After the collision of the aggregate, the remaining bonds were counted. The ratio of coordination number ζ/ζ_0 was used to express the degree of aggregate damage. The value of ζ/ζ_0 is defined as the average coordination number of all primary particles in the aggregate after the impaction to the initial average coordination number of primary particles in the aggregate before the collision. The coordination number was first applied to study impaction of complex structures by Kafui and Thornton (1993). Also, for generated fragments or restructured aggregates after impaction, the ratio between average value of radius of gyration of fragments to the initial value of radius of gyration of aggregate before collision is used. $\langle R_g \rangle / \langle R_{g,0} \rangle$. $\langle R_g \rangle$ was calculated by averaging R_g values over all developed fragments after the impaction and $\langle R_{g,0} \rangle$ was obtained by averaging the initial value of $R_{g,0}$ before collision over all generated aggregate structures.

Fragmentation here is defined as a split of aggregate into two or more than two often unequal parts, which leads development of new smaller aggregate structures. Eviction here is defined as an escape of a single particle from the structure of aggregate during its collision with rigid surface. Eviction is a particular case of fragmentation. Resistance of aggregate against breakage here is defined by the value of the critical distance between neighbouring primary particles.

Strength of connections between primary particles can be obtained using Eq. (6), (Przekop et al., 2004). Spring constant between two neighbouring particles was calculated using Eq. (6) where κ_s was calculated using Eq. (8). Eviction of primary particle from aggregate structure is available when particle will produce sufficiently large oscillation energy to break the connection with the closest neighbouring particles during an impaction. Large particle oscillations result in exceeding the critical distance between connected particles. When the critical distance between primary particles is exceeded, the bond between particles breaks and particles become separated. This means that bond (spring) force is not calculated any more for those particles. Also, all tee and both quadruple configurations involving this separated pair of particles will be neglected in calculations.

One can obtain the critical (maximum) distance at which a bond between two particles breaks, by analyzing relations between the applied force, contact radius and approach, defined as a difference between particle radius and the distance from the particle centre to the contact surface (Ziskind et al., 2000):

$$y_{cr} = 2\left[\frac{d_p}{2} + 0.437\left(\frac{\pi^2\gamma^2\frac{d_p}{2}}{\kappa_s^2}\right)^{1/3}\right] \tag{28}$$

The value of the critical distance y_{cr} depends strongly on the parameters Y, ν and γ. Therefore, for different values of k_s, the values of y_{cr} and f_{pp} will vary. After the particular bond is destroyed, all the tee and quadruple configurations associated with that bond also will be destroyed.

On the other hand, in case when two particles approach each other at the distance less than diameter of primary particles, those particles are considered to create a new bound, according to short-range van der Waals forces (Becker et al., 2009). Newly bonded particles are joined by spring–damp system, described by Eq. (5). The rest of the configurations (tee, quadruples) will be generated with that developed new bond.

Cases used in the numerical investigation are listed in Table 1. Process parameters are given in Table 2.

Table 1. Investigated cases of aggregates during numerical simulation of impaction

Case	γ_p [Jm^{-2}]	k_s [kgs^{-2}]	k_b [kgs^{-2}]	k_{ub} [kgs^{-2}]	k_t [kgs^{-2}]	k_p [kgs^{-2}]	d_p [nm]	D_f
1	0.15	35.2940	10^{-24}	0.05	2×10^{-24}	2×10^{-26}	5	2.20
2	0.20	38.8461	10^{-24}	0.05	2×10^{-24}	2×10^{-26}	5	2.20
3	0.40	48.9429	10^{-24}	0.05	2×10^{-24}	2×10^{-26}	5	2.20
4	0.15	56.0255	10^{-24}	0.05	2×10^{-24}	2×10^{-26}	10	1.34
5	0.15	56.0255	10^{-24}	0.05	2×10^{-24}	2×10^{-26}	10	2.20
6	0.15	88.9346	10^{-24}	0.05	2×10^{-24}	2×10^{-26}	20	1.10
7	0.15	88.9346	10^{-24}	0.05	2×10^{-24}	2×10^{-26}	20	1.60
8	0.15	88.9346	10^{-24}	0.05	2×10^{-24}	2×10^{-26}	20	1.80
9 (flexible)	0.15	88.9346	10^{-29}	0.0001	2×10^{-24}	2×10^{-30}	20	2.20
10 (semiflexible)	0.15	88.9346	10^{-24}	0.05	2×10^{-24}	2×10^{-26}	20	2.20
11 (semi-stiff)	0.15	88.9346	10^{-21}	0.5	2×10^{-22}	2×10^{-22}	20	2.20
12 (stiff)	0.15	88.9346	10^{-19}	1	2×10^{-20}	2×10^{-21}	20	2.20

Table 2. Process parameters used in impaction simulation

Parameter	Value
ρ_p [kgm^{-3}]	2600
ρ_s [kgm^{-3}]	2600
Y_s [Pa]	2.15×10^{11}
Y_p [Pa]	8.01×10^{10}
ν_s [–]	0.29
ν_p [–]	0.27
γ_p [J·m^{-2}]	0.15; 0.20; 0.40
γ_s [J·m^{-2}]	0.15
U [m·s^{-1}]	0.1–200

During the impaction, an aggregate can i) remain unchanged preserving its initial appearance, ii) can be restructured often to another more compact structure, or iii) can undergo fragmentation. Therefore, three

different regimes can be distinguished. The scenario depends on the imposed impact velocity, internal parameters defining bonding and fractal appearance of aggregate. Note that although the restructured aggregate is one which possesses the same amount of primary particles after the impaction and before the collision, its internal structure can be modified. Damaged or fragmented aggregate is one, which lost at least 1 particle or was split into two or more fragments during impaction event.

Impact collision of fractal-like aggregates was simulated numerically using flexible aggregate model (FAM). Aggregate structure movement was obtained by integration of Eq. (3) by Verlet position algorithm, which gives stable numerical integration. Time step used to integrate the equations of motion was equal to $\Delta t = 110^{-12}$ s. The value of f_{pp} was approximated by Eq. (11) and the value of f_{ub} was chosen to be equal to $f_{pp}/100$. Before the collision, the values of individual terms of the forces are close to zero because the system of connected particles is in equilibrium. During the collision, when aggregate structure is beginning to be compressed (at the very beginning of collision), some particles experience greater forces (for example at the bottom of the aggregate structure) than other particles located at the top of the structure. Secondly, individual stretching force between pairs of joined particles will depend on the distance between connected particles and torsion, while bending forces will depend on appropriate angles. Therefore it is hard to point out which forces contribute to the movement of particles. During the collision, forces in some particle configuration might be grater that the other terms, for example bending forces of the referred configuration of particles, can be smaller than stretching forces at one time, while in another configuration of particles in aggregate, those forces can change rapidly. It would be a huge overestimation or underestimation to predict, which of the force terms in Eq. (3) is dominant, in such a complex system as fractal-like aggregate.

Interaction forces between surface particles and particles of aggregate were included at the deposition event. When an aggregate particle touches a particle located at the surface, a bond between those particles is generated, which could be also broken when critical distance is exceeded. Interaction forces between aggregate particles and surface particles were obtained using Eq. (5). Spring constant was calculated using Eq. (6) where κ_s was calculated using Eq. (8) as a function of Young modulus and Poisson ratio. In case of torsion, bending or other forces, constant values of stiffness coefficient were assumed. They were chosen arbitrarily in an appropriate range to alter the values of stiffness coefficient in these forces, in order to gain different physical properties of aggregate populations. The types of models based on potential energy functions presented for example by Isella and Drossinos (2011), included bending term only. Paszun and Dominik (2009) estimated the rolling energy between neighboring particles by critical displacement. The surface energy between primary particles of aggregate and surface particles was obtained using Eq. (7). Determination of damping force and damped oscillations between surface and aggregate particles was conducted with:

$$F_i^{dps} = -f_{ps}\nu_i \tag{29}$$

where f_{ps} was estimated from Eq. (11). Brownian force and hydrodynamic drag force of the fluid were neglected, as aggregates moved in vacuum conditions.

3.1. Restructuration and fragmentation of aggregates as a function of spring constant, k

To investigate the strength of the bond between primary particles, expressed by the bond constant, k_s, on the restructuration and fragmentation process of aggregates, three different k_s values, cases 1, 2 and 3 were used. Value of k_s is a dependent variable, and it dependents on three other arguments according to Eq. (6). A greater value of k_s is achieved by imposing here a greater value of γ_p, keeping other values constant.

As one can observe, the deformation of the aggregate structure depends on the strength of bonds between primary particles. When a greater value of k_s is imposed, the aggregate structure becomes more resistant to breakage. Comparing the average value of radius of gyration for cases 1, 2, 3, one can see that aggregates with higher k_s value (higher γ_p) have a higher average value of $\langle R_g \rangle / \langle R_{g,0} \rangle$, Fig. 4. This can be explained

by the fact that F_i^s value acting on i-th particle during its oscillations is linearly proportional to the value of k_s. Additionally, one can take into account the fact that with increase of a value of γ, the right-hand side of Eq. (28) has a greater value. Therefore, the critical distance that is required to break bonds between two particles has a greater value. For small impact velocities, aggregates did not fragment at all, and value of the ratio $\langle R_g \rangle / \langle R_{g,0} \rangle$ was constant. The smallest aggregates were produced after the collision with the highest impact velocities, between 70 and 200 m/s.

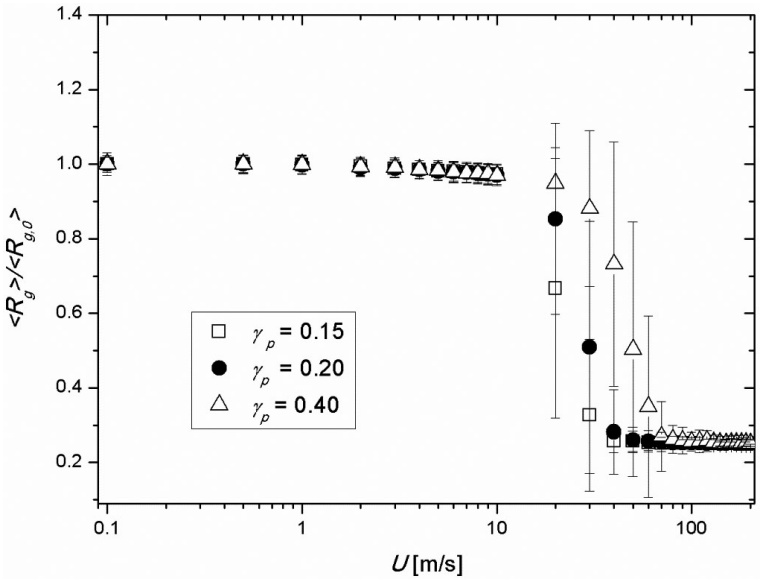

Fig. 4. Ratio of average radius of gyration to initial radius of gyration $\langle R_g \rangle / \langle R_{g,0} \rangle$ as a function of impact velocity. Aggregates from cases 1, 2, 3

Looking at the standard deviation bars, one can see that they are the largest between impact velocity in the range of 20–70 m/s. In that range of velocities, aggregates are restructured or can be fragmented. This can be compared to experimental results delivered by Ihalainen et al. (2012), who observed that aggregates, for some particular impact velocities, can generate smaller aggregates with different sizes or quite opposite, aggregates can be restructured. This is why standard deviation bars will overlap each other for a particular impact velocity.

Aggregates with a higher value of γ_p, must be conveyed with higher impact velocity towards the surface, in order to break bonds between joined particles, to achieve the same damage degree of breakage as aggregates with a lower value of γ_p. Looking at the coordination number plot, Fig. 5, one can see that aggregates with a higher value of γ_p have a higher average ratio of coordination number for impact velocities greater than 10 m/s. Therefore bonded primary particles with higher γ_p, after the impaction, preserve much more neighbouring particles than bonded particles where γ_p is lower. Results are similar to work presented by Moreno-Atanasio and Ghadiri (2006) who showed that aggregates were more resistible to breakage when surface energy between connected particles increased.

One can also observe that after the aggregate hits the surface with high impact velocity, primary particles are still connected. This is consistent with results reported by John and Sethi (1993) who investigated impaction of doublets with high impact velocities, and showed that particles can be still connected after impaction with high value of impact velocity.

In case when impact velocity is very high, k_s value does not control fragment sizes. One can suppose that lines will merge into one line at some particular impact velocity, Fig. 5.

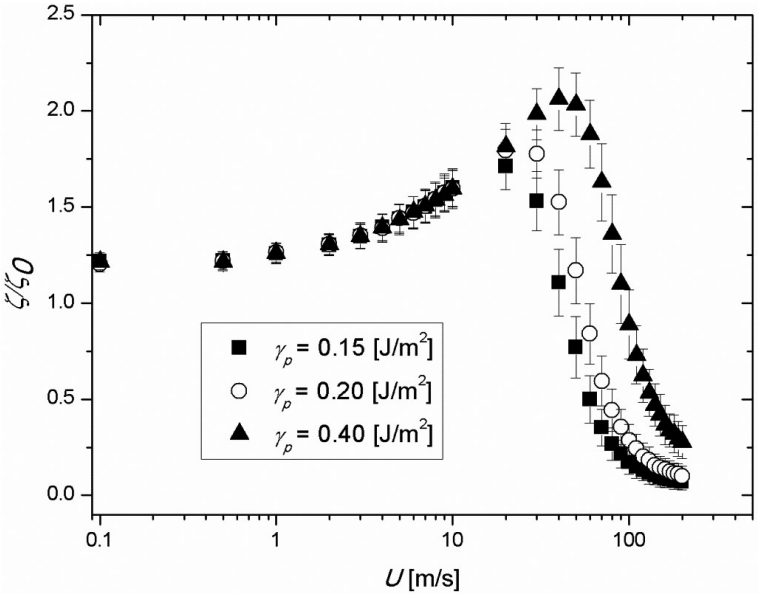

Fig. 5. Ratio of average coordination number ζ/ζ_0 relative to surface energy. Aggregates from cases 1, 2, 3

One can also see, in Fig. 5, a characteristic pick, which is connected with restructuration of aggregates to more compact structures. This will be commented later on in the section regarding impact of aggregates relative to their stiffness.

3.2. Restructuration and fragmentation of aggregates as a function of primary particle diameter

Aggregates with three different diameters of primary particles were analysed, with imposed parameters according to cases 1, 5 and 10.

One can observe that the structure of an aggregate is more resistant to breakage when the aggregate is composed of smaller primary particles, Fig. 6. Observing the plot, one can see that aggregates composed

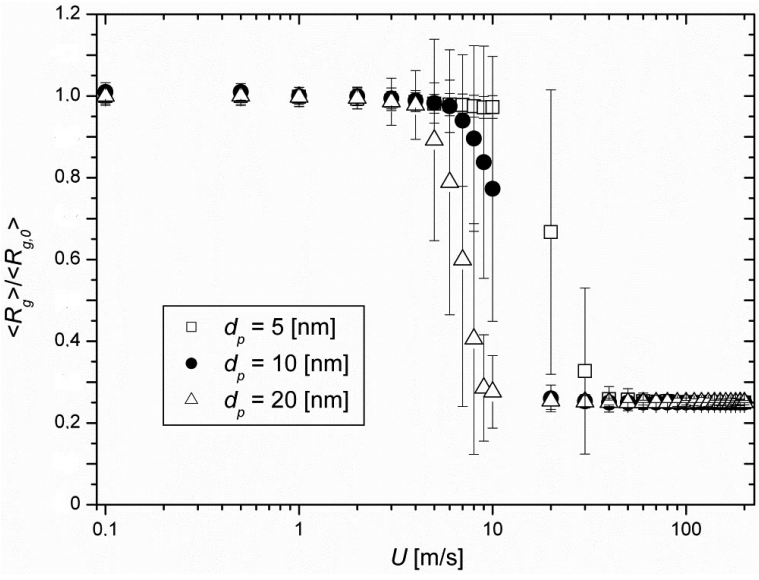

Fig. 6. Ratio of average radius of gyration to initial radius of gyration $\langle R_g \rangle / \langle R_{g,0} \rangle$ as a function of impact velocity. Aggregates from cases 1, 5, 10

of smaller primary particles produced the average $\langle R_g \rangle / \langle R_{g,0} \rangle$ value greater than aggregates composed of larger primary particles in the range of impact velocities between 7 and 30 m/s. It is not trivial to explain the results. The results are strongly connected with the value of the spring constant, k_s. Several factors may play a role here. Mathematically, with increasing diameter of primary particle of aggregate, the k_s value increases as well, according to Eq. (6). This should indicate that aggregates composed of larger primary particles are more resistive to breakage. However, bigger aggregates are composed of primary particles with bigger mass. Therefore at the impact event, bigger primary particle has greater kinetic energy, which produces larger oscillations with neighbouring particles. Therefore more massive primary particles are evicted easier from the structure of aggregate.

Those results are consistent with the work of Froeschke et al. (2003) and Seipenbusch et al. (2007) who reported that aggregates composed of smaller primary particles are harder to break. One should look also at standard deviation bars, which indicate that the aggregate with smaller primary particles can be more damaged after collisions, than aggregate that was composed of bigger primary particles. As explained before, aggregates that are impacting with middle impact velocities generate different sizes of fragments each time they hit the surface and the impact pattern is hardly repeatable (Ihalainen et al., 2012).

Observing the coordination number one can see that aggregates composed of smaller primary particles have higher average ratio of coordination number after the impaction, Fig. 7. This indicates that aggregates composed of smaller primary particles after the impaction are more resistant to breakage. Those aggregate primary particles are connected with more neighbouring particles after the impaction, compared to aggregates composed of bigger constituents for specific impact velocity.

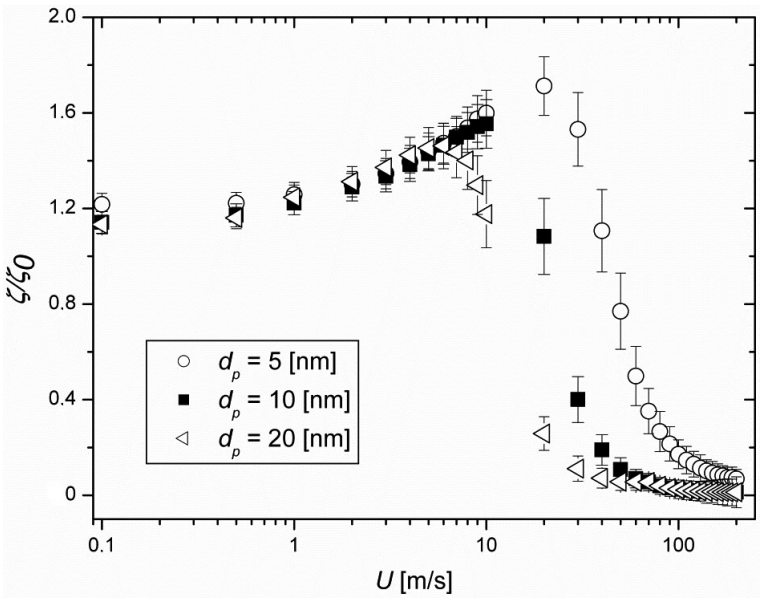

Fig. 7. Ratio of average coordination number ζ/ζ_0 as a function of impact velocity. Aggregates from cases 1, 5, 10

One can observe that, for very high impact velocities, the average ratio of coordination number is equal to zero. This is due to the fact that, after impaction with very high impact velocities, aggregates are split into single particles. Coordination number of a single particle is equal to zero.

3.3. Restructuration and fragmentation of aggregates as a function of fractal dimension

The simulation performed employed aggregates with different fractal dimensions according to parameters from cases 6, 7, 8 and 10. As the results indicate, restructuration and fragmentation of aggregate structure

was hardly influenced by its fractal dimension D_f, Fig. 8. However, one can see some differences. One can observe that aggregates with higher fractal dimension after the impaction had a greater value of ζ/ζ_0. This can be explained by the fact that aggregates with higher D_f are composed of primary particles which have higher coordination number, compared to aggregates with lower D_f. Subsequently it is harder to evict from the structure a particle which has a larger amount of neighbouring particles.

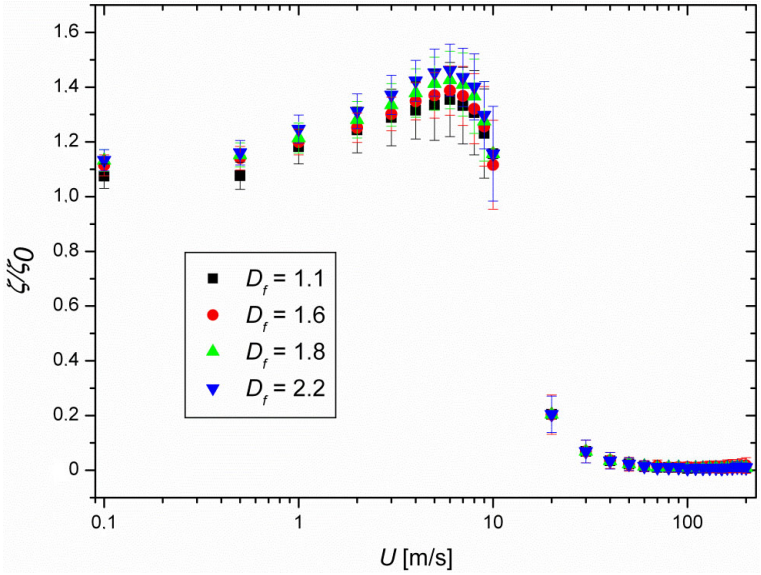

Fig. 8. Ratio of average coordination number ζ/ζ_0 in dependence of fractal dimension of aggregate. Aggregates from cases 6, 7, 8, 10

Small differences between particular aggregates for different impact velocities can be related to the material properties of primary particles. However, one can see some differences between average values of ζ/ζ_0 for aggregates with different D_f for medium impact velocities. In this range of velocities more compact aggregates have final average value of ζ/ζ_0 greater than more open aggregates. This is related to the fact that primary particles making up aggregates with higher D_f have shorter distances to other neighbouring particles, compared to aggregates that are more open, where distances between primary particles are greater.

As the impact velocity increases, differences between aggregates with different fractal dimensions disappear.

The results are consistent with Froeschke et al. (2003), who reported that aggregates with higher D_f are more resistant to breakage. Results presented here show as aggregate D_f increases aggregates develop even more compact structures for some impact velocities after the impaction. Therefore aggregates with $D_f = 2.2$ are more resistant to breakage than aggregates with $D_f = 1.1$.

3.4. Restructuration and fragmentation of aggregates as a function of impact velocity

The aggregate dynamical behaviour was investigated in the range of impact velocities between 0.1–200 $\mathrm{m{\cdot}s^{-1}}$. As results indicate, impact velocity determines when the aggregate structure remains unchanged, becomes restructured or damaged.

Observing Fig. 7, one can see that although the aggregate ratio of coordination number increased, it remained almost the same for impact velocities 0.1 and 0.5 m/s. Increased value of ζ/ζ_0 is explained by the fact that during the impaction of aggregate some primary particles were bonded together unavoidably

especially at the bottom of the structure, increasing the average ratio of ζ/ζ_0. The same aggregate structure behaviour was observed after numerical experiments processed by Ilmura et al. (1998) which also showed slight modification of aggregate structure toward bottom after the impaction with small velocity. Looking at the plot of $\langle R_g \rangle / \langle R_{g,0} \rangle$ value in dependence of impact velocity one can see that ratio $\langle R_g \rangle / \langle R_{g,0} \rangle$ is constant for the smallest impact velocities, Fig. 6.

As the impact velocity increases, the aggregate undergoes restructuration. Looking at the value of $\langle R_g \rangle / \langle R_{g,0} \rangle$ which slightly decreases, Fig. 6, one can judge that aggregates are modified to more compact shapes. This is proved as well by observing ratio of coordination number plot, Fig. 7, the value of which is increased for particular impact velocity. After the impaction, primary particles have greater amount of neighbouring particles than before the impaction. It should be noted that the degree of aggregate structure modification is influenced by the stiffness of structure, which will be explained in the next section.

Further increase in the impact velocity of aggregates results in producing more damaged aggregates. One can observe an alteration from restructuration regime to fragmentation regime, as the ratio of average coordination number suddenly decreases, Fig. 7. The boundary between those two regimes can be different, depending on the fractal appearance of aggregate, the bond strength and the primary particle diameter of an aggregate. At the fragmentation regime when the aggregate hits the surface, its structure can be split into several smaller child aggregates, or the aggregate can experience erosion, where a few of primary particles escape the structure, leaving bigger unregimented chunk of the aggregate structure behind. The aggregate can be also split into two large fragments. A variety of fragment seizes developed after the impaction can be observed by looking at the standard deviation of aggregate fragments, in the $\langle R_g \rangle / \langle R_{g,0} \rangle$ plot as a function of impact velocity, Fig.6. In the fragmentation regime the aggregate may not experience any particle eviction or quite opposite it may be fragmented into smaller aggregates with different sizes. These results were confirmed in experiments conducted by Ihalainen et al. (2012; 2014). Ihalainen et al. (2012) observed that aggregates can be fragmented or not at specific impact velocity.

In case when one increases the impact velocity further, aggregates become severely damaged. It can be seen in Fig.6 where the aggregate average $\langle R_g \rangle / \langle R_{g,0} \rangle$ value is a small value. Results reported here are in line with results reported by Froeschke et al. (2003), Rothenbacher et al. (2008) and with numerical simulations conducted by Grzybowski and Gradoń (2009) at fragmentation regime, who stated that when an aggregate hits the surface with greater impact velocity its structure becomes more damaged. Fragmentation of aggregates can be explained by the fact that, as the impact velocity increases, primary particles gain a greater value of oscillation energy, which is used to break bonds between them and their contact particles. For the highest values of impact velocities, one can see that the aggregate ratio of average coordination number is decreasing, Fig. 7.

3.5. Restructuration of aggregates as a function of their structure stiffness

The restructuration and fragmentation process of the aggregate structure is influenced by stiffness of the aggregate. Stiffness of the aggregate structure can be controlled in the model of FAM by four constants A higher value of the particular constant indicates that the particular configuration of particles in the aggregate structure is stiffer. When the value of one stiffness parameter would be increased, and the other stiffness parameter decreased, the aggregate will not be entirely stiff nor flexible, therefore it would be hard to correlate results with stiffness. Aggregates from cases 9, 10, 11 and 12 were used for simulation.

Observing Fig. 9, one can see that although the aggregate ratio of coordination number increased, it remains constant for impact velocities 0.1 and 0.5 m/s. This is due to the fact that during the impaction of aggregate some primary particles will be bonded, increasing the average ratio of ζ/ζ_0. As impact velocity is increased, the difference in value of the ζ/ζ_0 appears. Observing the ratio of coordination number at this

regime, one can see that as the aggregate structure is stiffer, the curve is closer to unity value, Fig. 9. One presumably cannot see the difference in ζ/ζ_0 for two cases, semi-stiff and stiff. The curves almost overlap each other. This was done to prove that small changes in the stiffness parameters influence the ζ/ζ_0 ratio.

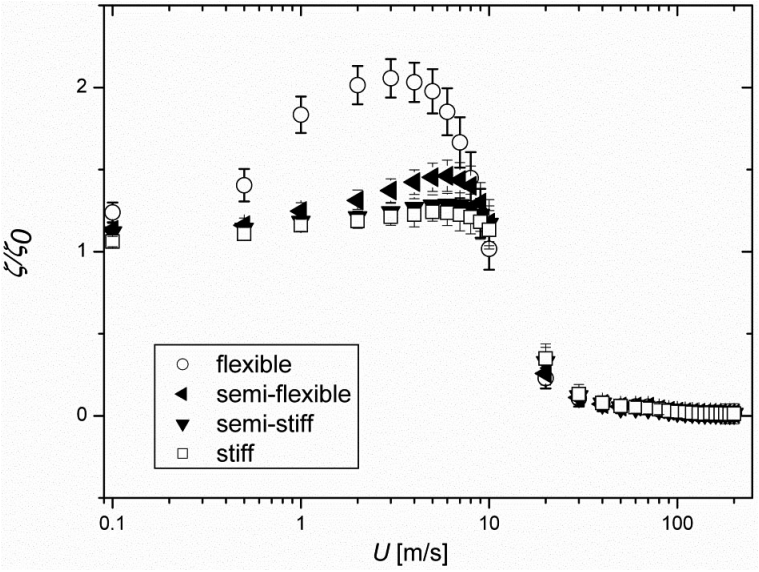

Fig. 9. Ratio of average coordination number ζ/ζ_0 as a function of stiffness of aggregate structure. Aggregates from cases 9, 10, 11, 12

As the aggregate become less stiff (lower values of stiffness parameters) the aggregate ratio of coordination number becomes higher. This indicates that less stiff aggregates become more compact in the restructuration regime after the impaction. For flexible aggregates, impact energy is transferred to deformation of their structure.

It should be emphasized that stiffness does not influence at which value of the impact velocity the aggregate will be fragmented.

Dominik and Tielens (1997) investigated soft dust colliding aggregates and found similar restructuration regime. One aggregate was conveyed to collide with another one. The authors recognized that aggregate structures remained unchanged when they collided with small impact velocities. When impact velocity exceeded critical, two colliding aggregates generated more compact structure after collision (restructuration regime), and when the impaction velocity of aggregates was very high, the aggregates became fragmented.

4. CONCLUSIONS

The evolution of aggregate structure after the collision with a rigid surface was investigated as a function of different strengths between contacting particles (described by bonding force), fractal dimensions D_f, diameter of primary particle of an aggregate and stiffness of the aggregate structure (described by different harmonic potential functions) the impaction velocity. The aggregate with increased strength of bonds between primary particles, with higher fractal dimension, composed of the smallest primary particles, represented a structure with the highest resistance to breakage. It was also found that the aggregate, depending on the impact velocity, showed three different dynamic behaviours. At the smallest impact velocities the aggregate experienced no change in its structure and ratio of coordination number was constant. As the impact velocity increased the aggregate could be restructured to another shape, remain unchanged or be fragmented, depending on the stiffness of the aggregate structure. Finally, the aggregate

could become fragmented, depending on the impaction energy, and could be split into fragments with different radius of gyration. Apart from ζ/ζ_0 value, one has to monitor $\langle R_g\rangle/\langle R_{g,0}\rangle$ ratio, because the $\langle R_g\rangle/\langle R_{g,0}\rangle$ provides more accurate information about post-collision morphology of fractal-like aggregates.

This work was financed by National Science Centre, Poland granted by decision number: UMO 2015/19/B/ST8/0599.

SYMBOLS

$\boldsymbol{A}$	normal vector of plane created by triplet of particles $i-j-k$
$\boldsymbol{B}$	normal vector of plane created by triplet of particles $j-k-l$
d_p	diameter of primary particle, m
C_C	Cunningham slip correction factor
D_f	fractal dimension
k_b	bending constant, kg·s^{-2}
k_p	inversion constant, kg·s^{-2}
k_s	bond constant, kg·s^{-2}
k_{ub}	Urey–Bradley constant, kg·s^{-2}
f_{pp}	damping factor, kg·s^{-1}
f_{ub}	Urey–Bradley factor, kg·s^{-1}
$\boldsymbol{F}^b$	bending force, N
$\boldsymbol{F}^{dpp}$	damping force, N
$\boldsymbol{F}_g$	gravity force, N
$\boldsymbol{F}^p$	inversion force, N
$\boldsymbol{F}^{ps}$	surface-particle interaction force, N
$\boldsymbol{F}^s$	bond (spring) force, N
$\boldsymbol{F}^t$	torsion force, N
$\boldsymbol{F}^{ub}$	Urey–Bradley force, N
r	position, m
r_0	equilibrium distance, m
R_g	radius of gyration, m
U	impact velocity, m·s^{-1}
v^{rel}	relative velocity, m·s^{-1}
V_b	cosine angle potential energy, J
V_s	bond potential energy, J
V_b	Urey–Bradley potential energy, J
Y	Young modulus, Pa
y_{cr}	critical distance, m

Subscripts

0	initial
i, j, k, l	denotes particles labelled i, j, k, l
p	denotes particle
s	denotes surface

Greek letters

γ	surface energy, J·m^{-2}
ζ	coordination number
Θ	angle, rad

κ_s	elastic constant, Pa
ν	Poisson ration
ξ	angle, rad
φ	angle, rad
ρ_p	particle density, kg·m^{-3}
μ	dynamic viscosity, Pa·s

REFERENCES

Allen M.P., Tildesley D.J., 1987. *Computer simulation of liquids*. Oxford Clarendon Press, New York.

Bałazy A., Podgórski A., 2007. Deposition efficiency of fractal-like aggregates in fibrous filters calculated using Brownian dynamics method. *J. Colloid Interface Sci.*, 311, 323–337. DOI: 10.1016/j.cis.2007.03.008.

Becker V., Schlauch E., Behr M., Briesen H., 2009. Restructuring of colloidal aggregates in shear flows and limitations of the free-draining approximation. *J. Colloid Interface Sci.*, 339, 362–372. DOI: 10.1016/j.cis.2009.07.022.

Cundall P.A., 1971. *The measurement and analysis of accelerations in the rock slopes*. Ph.D. thesis, Imperial College, London.

Cundall P.A., Strack O.D.L., 1979. A discrete numerical model for granular assemblies. *Géotechnique*, 29, 47–65. DOI: 10.1680/geot.1979.29.1.47.

Dai Q., 2010. Prediction of dynamic modulus and phase angle of stone-based composites using a micromechanical finite-element approach. *J. Mater. Civ. Eng.*, 22, 618–627. DOI: 10.1061/(ASCE)MT.1943-5533.0000062.

Derjaguin B.V., Muller V.M., Toporov Y.P., 1975. Effect of contact deformations on the adhesion of particles. *J. Colloid Interface Sci.*, 53, 314–326. DOI: 10.1016/0021-9797(75)90018-1.

Dominik C., Tielens A.G.G.M., 1997. The physics of dust coagulation and the structure of dust aggregates in space. *Astrophys. J.*, 480, 647–673. DOI: 10.1086/303996.

Ermak D.L., McCammon J.A., 1978. Brownian dynamics with hydrodynamic interactions. *J. Chem. Phys.*, 69, 1352–1360. DOI: 10.1063/1.436761.

Friedlander S.K., Jang H.D., Ryu K., 1998. Elastic behaviour of nanoparticle chain aggregates. *App. Phys. Lett.*, 72, 173–175. DOI : 10.1063/1.120676.

Friedlander S.K., 1999. Polymer-like behavior of inorganic nanoparticle chain aggregates. *J. Nanopart. Res.*, 1, 9–15. DOI: 10.1023/A:1010017830037.

Friedlander S.K., 2000. *Smoke, dust, and haze: Fundamentals of aerosol dynamics*. Oxford University Press, New York.

Froeschke S., Kohler S., Weber A.P., Kasper G., 2003. Impact fragmentation of nanoparticle agglomerates. *J. Aerosol Sci.*, 34, 275–287. DOI: 10.1016/S0021-8502(02)00185-4.

Gao G., 1998. *Large scale molecular simulations with application to polymers with nano-scale materials*. Ph.D. Thesis, California Institute of Technology.

Grzybowski K., Itoh H., Gradoń L., 2009. Restructurization of nanoaggregates in the impact breakage process. *Chem. Process Eng.*, 30, 99–110.

Guingo M., Minier J.P., 2008. A new model for the simulation of particle resuspension by turbulent flows based on a stochastic description of wall roughness and adhesion forces. *J. Aerosol Sci.*, 39, 957–973. DOI: 10.1016/jaerosci.2008.06.007.

Harada S., Tanaka R., Nogami H., Sawada M., 2006. Dependence of fragmentation behaviour of colloidal aggregates on their fractal structure. *J. Colloid Interface Sci.*, 301, 123–129. DOI: 10.1016/j.cis.2006.04.051.

Ilmura K., Nakagawa H., Higashitani K., 1998. Deformation of aggregates depositing on a plate in a viscous fluid simulated by a modified discrete element method. *Adv. Powder Techn.*, 9, 345–361. DOI: 10.106/S0921-8831(08)60565-8.

Ilmura K., Watanabe S., Suzuki M., Hirota M., Higashitani K., 2009. Simulation of entrainment of agglomerates from plate surfaces by shear flows. *Chem. Eng. Sci.*, 64, 1455–1461. DOI: 10.106/j.ces.2008.10.070.

Ihalainen M., Lind T., Torvela T., Lehtinen K.E.J., Jokiniemi J., 2012. A method to study agglomerate breakup and bounce during impaction. *Aerosol Sci. Techn.*, 46, 990–1001. DOI: 10.1080/02786826.2012.685663.

Ihalainen M., Lind T., Arffman T., Torvela A,. Jokiniemi J., 2014. Break-up and bounce of TiO_2 agglomerates by impaction. *Aerosol Sci. Techn.*, 48, 31–41. DOI: 10.1080/02786826.2013.852155.

Isella L., Drossinos Y., 2011, On the friction coefficient of straight-chain aggregates. *J. Colloid Interface Sci.*, 356, 505–512. DOI: 10.1016/j.cis.2011.01.072.

Johnson K.L., Kendall K., Roberts A.D., 1971. Surface energy and the contact of elastic solids. *Proc. Royal Soc. London A*, 324, 301–313. DOI: 10.1098/rspa.1971.0141.

John W., Sethi V., 1993. Breakup of latex doublets by impaction. *Aerosol Sci. Technol.*, 19, 57–68. DOI: 10.1080/02786829308959621

Kafui K.D., Thornton C., 1993. Computer simulated impact of agglomerate. In: Thornton C. (Ed.) *Powders & Grains 93, the Proceedings of the Second International Conference on Micromechanics of Granular Media*. A. Balkema, Rotterdam, pp. 401–406.

Moreno R., Ghadiri M., Antony S.J., 2003. Effect of the impact angle on the breakage of agglomerates: a numerical study using DEM. *Powder Technol.*, 130, 132–137. DOI: 10.1016/S0032-5910(02)00256-5.

Moreno-Atanasio R., Ghadiri M., 2006. Mechanistic analysis and computer simulation of impact breakage of agglomerates: Effect of surface energy. *Chem. Eng. Sci.*, 61, 2476–2481. DOI: 10.1016/j.ces.2005.11.019.

Pantina J.P., Furst E.M., 2005. Elasticity and critical bending moment of model colloidal aggregates. *Phys. Rev. Lett.*, 94, 138301. DOI: 10.1103/PhysRevLett.94.138301.

Przekop R., Grzybowski K., Gradoń L., 2004. Energy-balanced oscillatory model for description of particles deposition and re-entrainment on fiber collector. *Aerosol Sci. Technol.*, 38, 330–337. DOI: 10.1080/027868204904227669.

Reeks M.W., Reed J., Hall D., 1988. On the resuspension of small particles by a turbulent flow. *J. Phys. D: Appl. Phys.*, 21, 574–589.

Rennecke S., Weber A.P., 2013. The critical velocity for nanoparticle rebound measured in a low pressure impactor. *J. Aerosol Sci.*, 58, 135–147. DOI: 10.1016/j.jaerosci.2012.12.007.

Rothenbacher S., Messerer A., Kasper G., 2008. Fragmentation and bond strength of airborne diesel soot agglomerates. *Part. Fibre Toxicol.*, 5, 9. DOI: 10.1186/1743-8977-5-9.

Seipenbusch M., Toneva P., Peukert W., Weber, A.P., 2007. Impact fragmentation of metal nanoparticle agglomerates. *Part. Part. Syst. Char.*, 24, 193–200. DOI: 10.1002/ppsc.200601089.

Seipenbusch M., Rothenbacher S., Kirchhoff M., Schmid H.J., Kasper G., Weber A.P., 2010. Interparticle forces in silica nanoparticle agglomerates. *J. Nanopart. Res.*, 12, 2037–2044. DOI: 10.1007/s11051-009-9760-5.

Seizinger A., Speith R., Kley W., 2012. Compression behavior of porous dust agglomerates. *Astron. Astrophys.*, 541, A59. DOI: 10.1051/0004-6361/201218855.

Strobel R., Pratsinis S.E., 2007. Flame aerosol synthesis of smart nanostructured materials. *J. Mater. Chem.*, 17, 4743–4756. DOI: 10.1039/B711652G.

Tamadondar M.R., Rasmuson A., Thalberg K., Niklasson B.I., 2017. Numerical modeling of adhesive particle mixing. *AIChE J.*, 63, 2599–2609. DOI: 10.1002/aic.15654.

Thornton C., Yin K.K., Adams M.J., 1996. Numerical simulation of the impact fracture and fragmentation of agglomerates. *J. Phys. D: Appl. Phys.*, 29, 424–435. DOI: 10.1088/0022-3727/29/2/021.

Vainshtein P., Ziskind G., Fichman M., Gutfinger C., 1997. Kinetic model of particle resuspension by drag force. *Phys. Rev. Lett.*, 78, 551–554. DOI: 10.1103/PhysRevLett.78.551.

Walker P.M.B. (Ed.), 1988. *Chambers science and technology dictionary*. Chambers Harrap Publishers, London.

Wittel F.K., Carmona H.A., Kun F., Herrmann H.J., 2008. Mechanisms in impact fragmentation. *Int. J. Fract.*, 154, 105–117. DOI: 10.1007/s10704-008-9267-6.

Witten T.A., Sander L.M., 1981. Diffusion-limited aggregation, a kinetic critical phenomenon. *Phys. Rev. Lett.*, 47, 1400–1403. DOI: 10.1103/PhysRevLett.47.1400.

Zhang Y., Ma T., Luo X., Huang X.M., Lytton R.L., 2019. Prediction of dynamic shear modulus of fine aggregate matrix using discrete element method and modified Hirsch mode. *Mech. Mater.*, 138, 103148. DOI: 10.1016/j.mechmat.2019.103148.

Ziskind G., Fichman M., Gutfinger C., 2000. Particle behavior on surfaces subjected to external excitations. *J. Aerosol Sci.*, 31, 703–719. DOI: 10.1016/S0021-8502(99)00554-6.

Żywczyk Ł., Moskal A., 2015. Modelling of deposition of flexible fractal-like aggregates on cylindrical fibre in continuum regime. *J. Aerosol Sci.*, 81, 75–89. DOI: 10.1016/j.jaerosci.2014.12.002.

Received 15 July 2019
Received in revised form 21 November 2019
Accepted 25 November 2019